IJMT. Vol. 21, Iss. 1, 2025. (1-11)

International Journal of Maritime Technology

Journal homepage: ijmt.ir

Propeller connection to diesel engine in two shaft line designs of a catamaran passenger ship

Mojtaba Pakian Bushehri [1]

[1] *PhD in Mechanical Engineering, SMI Bushehr Shipyard; Pakianm@chmail.ir*

ARTICLE INFO

Article History:
Received: 3 Dec 2024
Last modification: 17 Feb 2025
Accepted: 11 Feb 2025
Available online: 11 Feb 2025

Article type:
Research paper

Keywords:
Matching of Propulsion System
Diesel engine
Propeller
Overload
Over speed

ABSTRACT

The engine braking power moves the ship and it is converted into effective power by taking into account the propulsion power losses and the propeller efficiency. The braking power diagram must be in a suitable position relative to the continuous power diagram and the maximum power of the engine to ensure safe engine operation. In this paper, the propulsion system of a catamaran passenger vessel is investigated and the matching condition of the propulsion components in two shaft line designs and their impact on the performance of the engine and vessel are analyzed in detail. The hull is subjected to CFD analysis and the resistance is calculated. Then, using the hydrodynamic coefficients of the propeller, the matching calculations of the propeller to the engine have been done. To match the propulsion system, the gearbox with 2.963:1 was coupled with the shaft line. The shaft line design is satisfactory in ship maneuvering and diesel engine performance. The ship's resistance was calculated by STAR-CCM+ software, used in matching calculations and the results have been validated by sea trials. The error between sea trial and matching calculations is a maximum of 7%.

ISSN: 2645-8136

DOI: http://dx.doi.org/10.61882/ijmt.21.1.1

1. Introduction

Connecting a propeller to engine and hull of a vessel is essential in analyzing the propulsion system and is a concern for ship designers. Matching a propeller to the gear ratio and engine means that the equilibrium between the available engine torque and the required propeller torque and the propeller can provide the required thrust.

This is the law of energy conservation that the engine power with considering the percentage of propulsion system drop must be equal to the power absorbed by the propeller [1]. Not matched propulsion system will result in overload or over speed in the diesel engine. In an overload engine, the RPM does not increase and additional load is applied to the engine. In over speed, if engine is not controlled by the Governor, RPM will be increased beyond the final RPM and the propeller cannot absorb all power of the engine [2]. Matching condition of propulsion is very effective because of the fuel consumption, and stress vibrations that may be caused by the loaded engine or the ship movement on the waves [3]. "To optimize the system, the following parameters must be considered, type of propulsion, maneuverability, fuel consumption, payload, main dimension, passenger/crew comfort, effects on the maritime environment, initial investment cost and so forth. But often, the initial investment cost becomes the major decision factor, while factors such as the life cycle perspective, the total fuel bill, and the total environmental impact over the ship's lifetime are given less attention" [4]. The propeller graph shows the performance of the ship based on engine loading at the optimal speed [5]. In the design and calculation of the propulsion system, it is necessary that the thrust of propulsion system overcomes total resistance at several speeds. The output power is the power driven by the shaft power and the shaft power is generated by the engine breaking power [6]. Hydrodynamic properties of the propeller are one of the most important parameters in design of the shaft and propeller propulsion system. Matching of the propulsion system means success in adaptation of the propeller, gearbox and engine which must match to the hull of the vessel. Marco et al. investigated the matching of the propulsion system to fuel consumption. They focused on calculating the optimal pitch for matching and achieving reduced fuel consumption. They developed a numerical code in MATLAB to perform the matching calculations [7]. Piano worked on the speed controlling as well as the position of marine vehicles. They focused on thrusting and controlling the propeller [8]. Habibi and Nurhadi investigated the 600 GT Ferry for the slow speed. They analyzed the propulsion system matching to select the correct type of B series propeller for the ship by using the Match program with a database of the propeller and marine engine [9]. They found that the most efficient propeller is B444. Ogar et al. performed an optimal matching of a controllable pitch propeller to the hull and diesel engine of the combine diesel or gas (CODOG) system in a frigate vessel. A matching program was used to obtain the matching point. The graphs showing the results were used to determine the matching point at the appropriate speed and power [10]. Nourhadi et al. studied the engine propeller matching for high-speed vessels with Gawn series propeller. They found out that in rough hull at 28 knots, the propeller had a performance of 0.56 and with the CAT 280-8 engine at 1000 rpm, the ship's speed reach 30.5 knots [11]. Gagro et al. investigated the feasibility of a propeller analysis based on a boundary layer method used in the propulsion optimization process to select and analyze the propeller performance under different maneuvering conditions. After the simulation validation in a diagonal flow, the analysis is extended to the two propellers of a ship [12]. Pakian bushehri and Golbahar haghighi investigated the matching of the surface-piercing propeller torque with the engine torque in an ambulance boat. They studied two motion of the boat, pre- planing stage and post- planing stage [13]. In another study, Pakian Bushehri and Golbahar haghigi investigated the effect of the gear ratio on the matching of the propulsion system of a catamaran [14]. Tran and Kim presented a new approach to engine, hull, and propeller adaptation under service conditions. This study was used to solve the adaptation problem of the tanker Glory Star. All results obtained were consistent with published actual experimental data for this ship with a power loss of 21.5% in service conditions [15]. Tan et al. investigated the effect of shaft line arrangements on the matching of the propulsion system. Using CFD, they investigated the effect of changing the axis tilt angle and distance between the twin axis [16]. Bayraktar et al. investigated propellers for connection to the main engine of a flying boat for speeds of 20 knots. Propeller designs were examined with the prediction of the resistance of the boat. The analysis shows that the P4, P7 and P9 propellers are closest to the performance chart and as long as advance coefficients are followed, the P4 propeller produces reliable results [17]. Ramadhan et al. investigated the connection of C5-75 and MAU4-65 propellers to the main engine to convert a Ro-Ro Vehicle Carrier into a Ro-Ro Passenger Ship. They examined the performance of these propellers for a speed of 21 knots in two hull conditions: clean and dirty. Propeller-to-engine matching calculations indicate a good match for the 12640 kW engine at 109 rpm (clean hull) and 112 rpm (dirty hull) [18]. In this paper, a practical comparison of the effect of two shaft line designs on the performance of a catamaran passenger ship has been done. Also, the effects of this point on the performance of the diesel engine for the maximum of service speed and top speed, acceleration reserve and efficiency of propulsion system have been investigated. The ship resistance is one of the most important parameters of propulsion system matching that it has been obtained by CFD analysis for the nine-ship speed.

2. Material and methods

This paper investigates the propulsion system of a passenger catamaran ship. In the first design, mismatching in the propulsion system caused overload in the engine. Then, in order to remove the overload, the design of the new propulsion system was examined. The passenger ship in this research is a catamaran vessel with a capacity of 220 passengers. Figure 1 shows the view of the catamaran at the shipyard.

Figure 1. the catamaran at the shipyard

The main hull of the vessel is modeled in Rhinoceros software [19].

2-1. Main Specifications of the Vessel

The main specification of the catamaran is presented in Table 1.

Table1. Specification of the catamaran

Length (m)	Width (m)	Depth (m)	Draft (m)	Top speed (Knots)	Cruise speed (knots)
40.05	11.46	3.9	1.8	20	30

2-2- Propulsion System Arrangement

The vessel has two engines with the power of 1680 kW and the gearboxes have a reduction ratio of 2.571: 1 and located in two demi hull of the vessel. The view of shaft line is shown in Figure 2. The angle of the propulsion installation is 4.7 °.

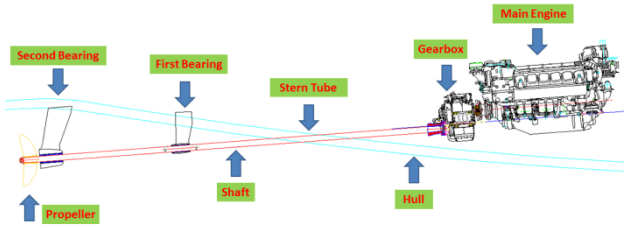

Figure 2. Plan of the shaft line

The shaft diameter is 110 mm that connected to the gearbox reduction ratio of 2.5: 1. The propeller is a fixed pitch propeller and the specification of propulsion system presented in Table 2. Figure 3 shown the drawing of the propeller.

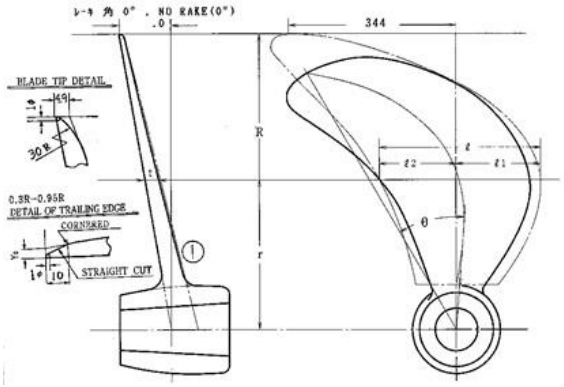

Figure 3: The drawing of the propeller

Table 2. Specification of propulsion system

Propeller diameter (m)	1.219
Propeller pitch (m)	1.524
No. Blade	5
DAR	1.05
Engine rpm	2000
Engine power (kW)	1680
Reduction ratio	2.571:1

2-3. Sea trial

The results of two shaft lines have been obtained in two sea trials. The second sea trial was done after changing the shaft line and the propulsion system equipment. The sea trials were done on calm sea and wind speed of 7 km/h.

2.4. CFD calculation

In order to obtain the resistance of the hull, the ship hull was analyzed in STAR-CCM+ software by CFD method [20]. The simulations are performed at nine different speeds of 7, 12, 16, 18, 20, 23, 25, 28, and 30 knots considering the ship two degrees of freedom, heave, and pitch motions of the ship. Numerical simulation is performed at speeds that are close to the points of the matching calculation. Figure 4 shows the computational domain with boundary conditions [21]. The symmetrical boundary condition is selected for two longitudinal sides of tank. Figure 5 shows the meshed model. The CFD calculations are performed in the domain with 5.81*E6 cells. The hexahedral mesh is selected for simulation. The boundary layer mesh is the prism layer type. The mesh independence is performed by the model resistance at 20 knots at different numbers of computational grids and is presented in Figure 6. It is observed in Figure 6, the increasing the number of cells from 5.81E6 to 11.37E6, there are only 1% of error. Therefore, 5.81*E6 of cells are used in the computations. The number of prism layers and the stretch factor of the prism layer mesh are 20 and 1.15, respectively.

The wall function Y + has been more than 35 and less than 70 along the wetted area at the fine mesh. Figure 7 shows the Y + contour for demi-hull.

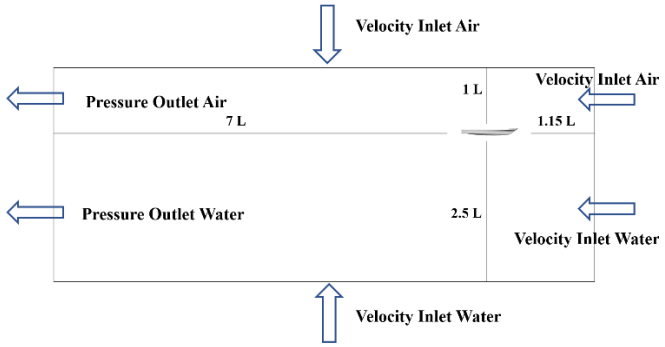

Figure 4. Computational Domain and Boundary Condition

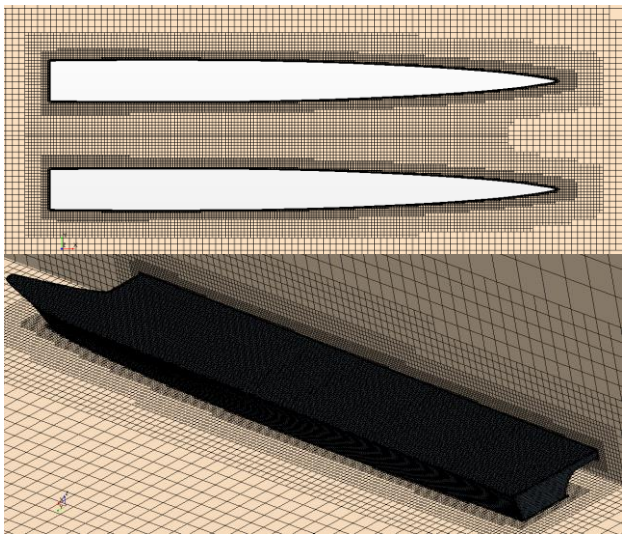

Figure 5. Computational mesh on the ship

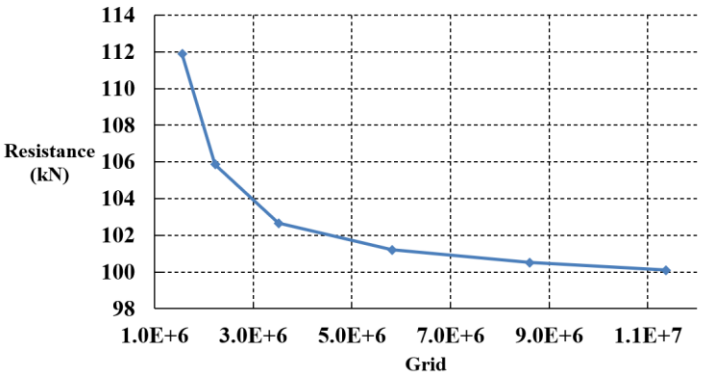

Figure 6. Mesh Independence Study

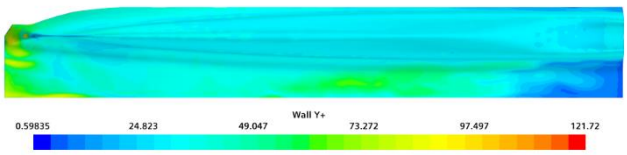

Figure 7. The Y+ contour

2.5. Governing Equations

The Navier Stokes equations are the governing equations of the fluid flow field. Navier Stokes equation is given in equation 1. It should be mentioned to simulate the resistance test (unsteady problem), Reynolds-averaged Navier–Stokes equations (RANS) need to be solved. Equation 2 shows the RANS equation. In the analysis of turbulent flow, due to the effect of turbulent motions, it is very difficult to solve them directly and for this reason, an appropriate turbulent model must be used as well as approximate terms. The presence of Reynolds stresses $\rho\overline{u_j'u_i'}$) add to the complexity of this issue. To solve such a problem, Reynolds stresses are modeled using viscosity models on linear vortices. For this purpose, linear equation 3 must be established.

$$\frac{\partial\vec{V}}{\partial t}+(\vec{V}\cdot\nabla)\vec{V}=-\nabla p+\nu\nabla^2\vec{V} \quad (1)$$

$$\rho\frac{\partial(U_i)}{\partial t}+\rho U_j\frac{\partial U_i}{\partial x_j}=-\frac{\partial p}{\partial x_j}+\frac{\partial}{\partial x_j}\left(2\mu S_{ji}-\rho\overline{u_j'u_i'}\right) \quad (2)$$

$$-\rho\overline{u_j'u_i'}=2\mu_t S_{ji}-\frac{2}{3}\rho k\delta_{ij} \quad (3)$$

In the above equations, Ui is the velocity vector. The t, p, and μ are time, pressure, and dynamic viscosity respectively. S_{ij} is the mean strain rate and u' is the component of velocity changes. Also, μ_t is called turbulent viscosity or vortex viscosity; k is turbulent kinetic energy and δ_{ij} is the Kronecker delta. According to the convergence of the equations, the K−ε model was applied as the turbulence model [22]. This turbulent viscosity model depends on turbulent kinetic energy (K) and turbulent dissipation rate (ε). K – ε turbulent model is represented in equation 4.

$$\mu_t=\rho C_\mu\frac{k^2}{\varepsilon} \quad (4)$$

The volume of fluid (VOF) method is used for the free surface of the sea. The isosurface is defined to display the water level. When the volume of water is reduced by half for each cell, it should be displayed as the free surface of the water. The solver model is selected implicit unsteady according to the software help for two-phase flow. The Eulerian multiphase is selected for materials.

In the calculation of propulsion system matching, the engine power graphs, specification of shaft line, and propeller hydrodynamic properties are required. The matching calculation must be performed for the hull with the propulsion system, so the resistance of the hull is required too.

Propeller speed, speed of advance, coefficient of advance, torque coefficient, thrust coefficient, propeller thrust, the horizontal component of thrust, delivery power, effective power, and efficiency of the

propeller are calculated using equations 5 to 14, respectively [23].

$$n_{prop} = {}^{n_{enge}}/_{Gear.r} \quad (5)$$

$$V_a = V_s(1 - W_T) \quad (6)$$

$$J = \frac{V_a}{n_{prop} * D_{prop}} \quad (7)$$

$$q = K_q * \rho * {n_{prop}}^2 * {D_{prop}}^5 \quad (8)$$

$$T = K_t * \rho * {n_{prop}}^2 * {D_{prop}}^4 \quad (9)$$

$$Del.T = T * T.Ded * 2 \quad (10)$$

$$Horiz.\ T = Del.\ T * Cos(Q) \quad (11)$$

$$P_D = q * n_{prop} \quad (12)$$

$$P_E = R_t * V_s \quad (13)$$

$$\eta = {}^{P_E}/_{P_D} \quad (14)$$

The approximate value of wake fraction and thrust deduction is calculated using the Taylor formula and Holtrop formula respectively. The selection of these regression- formulas is based on principal dimension of the vessel and the value of C_B. The equation 15 and equation 16 are presented the Taylor and Holtrop formula, respectively.

$$W_T = 0.55C_B - 0.2 \quad (15)$$

$$t = 0.325C_B - 0.1885\, D/\sqrt{BD_T} \quad (16)$$

Where D, B and DT are Propeller diameter, overall breadth of catamaran, and Draught respectively.

3. Results and discussion

The results are presented in four sub sections: the first sea trial, CFD analysis, matching calculations, and the second sea trial.

3.1. The first sea trial

Due to the presence of the gearbox with the gear ratio of 2.571:1 on the vessel, the first sea trial is performed with this gear ratio in the calm sea (wind speed of 7 km/h).

Table 3 shows the first sea trial results at the different speeds of the vessel. At this gear ratio, the top ship speed were 22 knots at 1600 rpm of the engine speed.

Table 4 shows the engine performance characteristics at 1600 pm. As is observed in Table 4, all engine parameters at 1600 rpm are natural and follow the manufacturer's request. Tcoolant is coolant temperature of freshwater of the engine and Tex.CombA, Tex.CombB is exhaust temperature to the left and right side of the engine respectively.

At this trial, the engine speed does not increase beyond 1600 rpm and when the engine speed is increased more than 1600 rpm and the secondary turbocharger is activated, the exhaust temperature of the engine is increased from 622 to 760 ° C. The results of the first sea trial showed that the engines are in an overloaded condition.

Table 3. The First Sea Trial Results

	n_{enge} (rpm)	n_{prop} (rpm)	Speed (knots)
١	600	233	7
٢	1200	467	16
٣	1400	545	18.5
٤	1600	622	22

Table 4. Engine Performance Characteristics at 1600 rpm

Test time	12:30		13:30	
	Port	Starboard	Port	Starboard
n_{enge} (rpm)	1600	1600	1600	1600
Tcoolant (° C)	78	78	79	78
Tex.combA (° C)	584	610	582	609
Tex.combB (° C)	608	635	615	634
Shaft Speed (rpm)	622	622	622	622
Speed (Knot)	22			

3.2. CFD Analysis

The resistance was calculated at speeds of 7, 12, 16, 19, 20, 23, 25, 28, and 30. For validation to numerical calculations, the resistance was calculated in the first sea trial. The resistance was calculated using the engine speed and ship speed in the first sea trial and using the propeller hydrodynamic characteristics diagram. The diagram of the hydrodynamic characteristics of the propeller is issued by the company. Resistance is equal to the horizontal component of thrust at different ship speeds. Therefore, formulas 5, 6, 7, 8, 9, 10, 11, 15 and, 16 have been used to calculate the resistance from the first sea trial. Table 5 shows the resistance calculation from the first sea trial. Figure 7 shows the comparison of resistance in CFD and the first sea trial. Table 6 shows the error between the resistance calculation of the CFD and the first sea trial. The maximum error is related to the speed of 16 knots, which is 15.5%. However, due to the difference in sea trial conditions and numerical simulation, simplification in calculations of wake fraction and thrust deduction, the error values are acceptable.

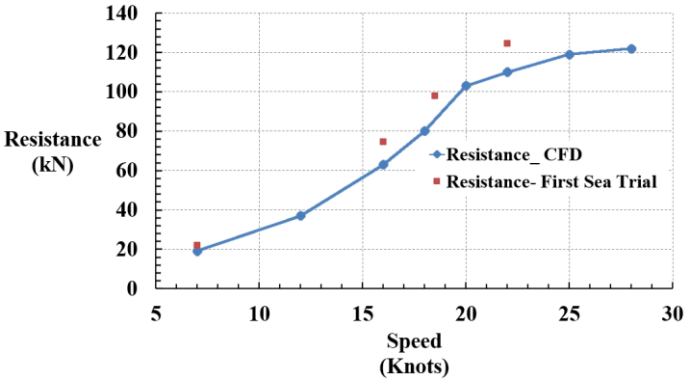

Figure 7. Resistance of Catamaran in CFD and First Sea Trial

Figure 8 shows the VOF contour at 20 knots. Therefore, VOF has been investigated during simulation to ensure the volume deduction of water. Figure 9 shows the wave contour.

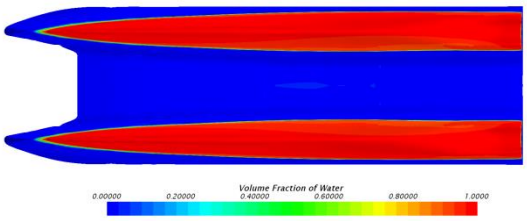

Figure 8. VOF contour at 20 knots speed of catamaran model

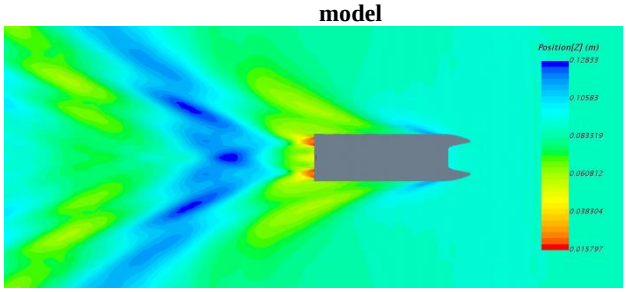

Figure 9. Wave contour at 20 knots speed

Table 5. Resistance Calculation from the First Sea Trial

n_{enge} (rpm)	Vs (Knots)	Va (m/s)	J	K_t	T (kN)	R_t (kN)
600	7	3.32	0.70	0.36	12.63	22.24
1200	16	7.65	0.80	0.30	42.18	74.59
1400	18.5	9.14	0.82	0.29	55.17	98.01
1600	22	10.64	0.84	0.28	69.88	124.79

Figure 10 also shows the comparison of the waveform contour with the sea trial. As can be seen, there is good accuracy between sea trial and CFD. As shown in Figure 10, there is a peak in the wave collision that grows with increasing speed.

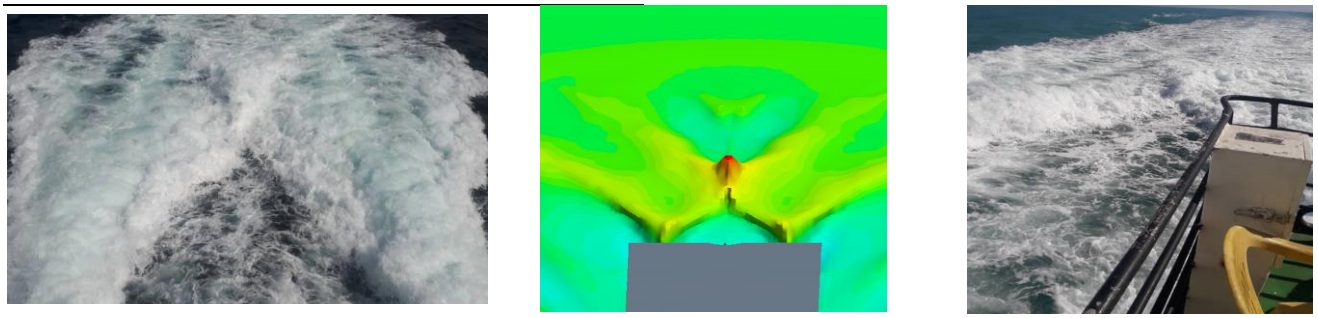

a b c

Figure 10. Comparison of the waveform: a- view from bridge of the vessel in sea trial, b- CFD analysis, c- view from the stern of the vessel in the sea trial

3.3. Matching calculation results

The engine used on the ship is MTU12V396. The power rating of the engine is 1680 kW at 2100 rpm and the speed limit is 600 to 2100 rpm. The maximum continuous rating (MCR) is 1400kW at 1975 rpm. Unit of fuel consumption in the graphs are g/kW.h. This engine is 1DS in the application group of MTU. So, the average load is ≤ 60% of rated power [24].

Tables 7 shows the matching calculations in case 1 (gear ratio 2.571:1) for different the engine speeds including the 600, 1000, 1200, 1400, 1600, 1800, 2000, and 2100 rpm. In matching calculation, ship speed is predicted at several engine speeds. The ship speed is calculated using the propeller pitch, propeller speed and prediction of slip. The horizontal component of the thrust of the propulsion system must be equal to the total ship resistance.

Table 6. The errors between the resistance calculation of the CFD and the first sea trial

	Vs (Knots)	Resistance –CFD (kN)	Resistance –Fist Sea Trial (kN)	Error (%)
1	7	19	22.2	14.5
2	16	63	74.5	15.5
3	18.5	88	98	10.2
4	22	110	124.7	11.7

Values of K_t and K_q were obtained by calculating the advance coefficient using equation 8 at the specific speeds. The approximate value of the wake fraction was obtained using the Taylor formula from equation 15. T/Prop is the thrust of one of the propellers calculated from equations 9 and Horiz. T is the horizontal component of the thrust of two propeller using equation 11. The approximate value of thrust deduction was obtained using the Holtrop formula from equation 16. q/Prop is torque of one of the propellers calculated from equation 8. P_D/Prop is the delivery power that one of the propellers consumes and can be obtained from equation 12; and Pb/Prop is the braking

power of the engine on each propeller and is calculated from delivery power by considering the power drop of the propulsion system. The design of this propulsion system is based on the LR standard [25]. There is a 4.5% drop power from the engine to a propeller that 3% for the gearbox and 1.5% to shaft bearings. T.Prop.Pow, Contin.Pow and Over.Pow are the propeller theoretical power, maximum continuous power, and overload power respectively. These values are presented in Table 7 and are selected from the Mtu12V396TE94 engine load diagram for 600 to 2100 rpm.

Matching calculations are performed for gear ratio 2.963:1. Figure 11 shows the Mtu12V396 load diagram and the design propeller power curve for each case. The engine load diagram presents the overload power limit (Over.Pow.Curve), the maximum continuous power (Contin.Pow.Curve), the propeller theoretical power (T.Prop.Pow), and speed limits. The design propeller power shows the braking power on each propeller (Pb/Prop). In 2.571:1, the design propeller power curve is tangent to the maximum continuous power curve from 600 to 1150 rpm and intersected at 1600 rpm. The point of intersection the design propeller power and MCR is the maximum range of continuous operation of the engine and the engine is unable to increase speed.

Table 7. Matching calculation at 2.571:1 of gear ratio

Engine rpm	Vs Knots	T/Prop N	Horiz. T N	q/Prop N.m	PD/Prop Kw	Pb/Prop (kW)	T.Prop.Pow (kW)	Contin.Pow (kW)	Over.Pow (kW)
600	7.8	11722	21145	2934.2	71.7	74.5	39	122	162
1000	13	30911.1	53913.1	7999.9	325.8	338.8	176	333	403
1200	16	42964.2	74679.4	11402.9	557.3	579.6	310	706	874
1400	19	54348.8	97768	15179.8	865.5	900.2	488	1013	1057
1600	23.6	65010.4	113386.7	17274.2	1125.7	1170.7	741	1167	1220
1800	28.7	70876.9	123618.6	19458.5	1426.5	1483.6	1050	1306	1411
2000	33	80654.3	140671.8	22492.4	1832.2	1905.5	1445	1400@1975	1620
2100	35.5	83888.1	146311.9	23417.46	2002.9	2083	1680	-	1680

The design propeller power curve of 2.963:1 has intersected the propeller theoretical power curve (T.Prop.Pow) near the 2000 rpm and then intersected the speed limit of engine and almost has intersected continues rating power at 2000 rpm. The MCR power is 1400 kW at 1975 rpm and the rating power is 1680 kW at 2100 rpm. The top ship speed will be 29 knots at 2100 rpm. In the design propeller power curve of case 1 (Pb.1), if the engine rating power was 2080 kW, the top speed will be 35.5 knots at 2100 rpm.

Figure 12 shows the propeller torque (Prop.Torque.Case1, Case2) and the torque after the gearbox (Torque.G.Case1, Case 2). The torque after the gearbox is obtained from the maximum engine torque at different engine speeds multiplied by the corresponding gear ratio. In other words, the torque after the gearbox is the torque transmitted by the gearbox. Torque.G.Case1 and Prop.Torque.Case1 corresponds to the gear ratio of 2.571:1. These graphs intersect at 18.7 kN of torque. Torque.G.Case2 correspond to the 2.963:1 of gear ratio. Both graphs don't have any contact and the maximum engine torque and propeller torque are 22.62 kN and 20.82 kN, respectively.

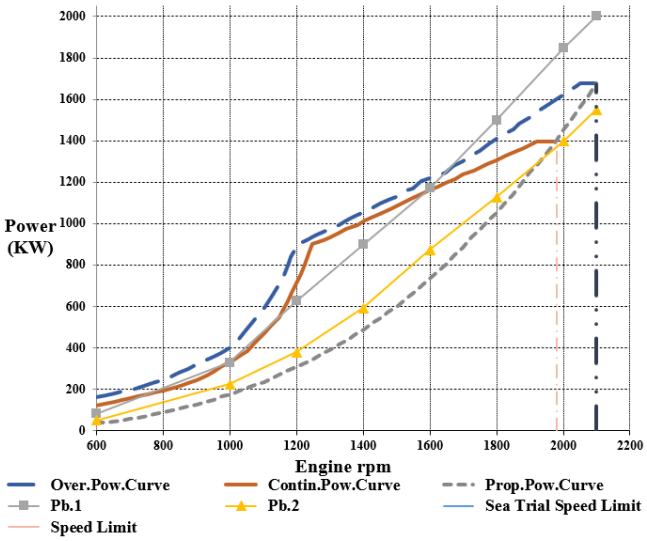

Figure 11. The curves of engine load diagram, the D.Prop.Pow.2.571:1, and D.Prop.Pow.2.963:1

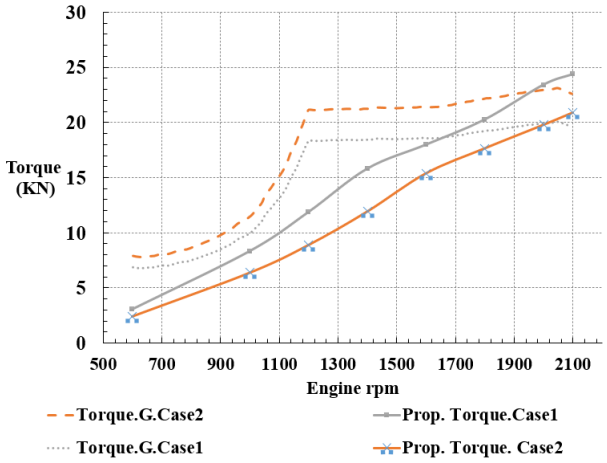

Figure 12. Propeller torque and delivered torque after the gearbox for all cases

Prediction of the ship speed is presented in Figure 13 at the several engine speeds in all cases. The ship speed is obtained from the propeller rotation speed multiplied by the propeller pitch and predicting the propeller slip. The values of propeller slip are well predicted by the first sea trial result. In case 1, the slope of the graph has increased at 1400 rpm, and in case 2, the slope has increased from 1600 rpm, respectively. The slope of graph is increased at propeller rotation speed of 540 to 585 rpm in two cases and shows a significant reduction in propeller slip for this range. It should be noted that the gear ratios of case 1 will not reach the top speed due to engine overload. The top speed of the ship is presented in Table 8 for the two gear ratios.

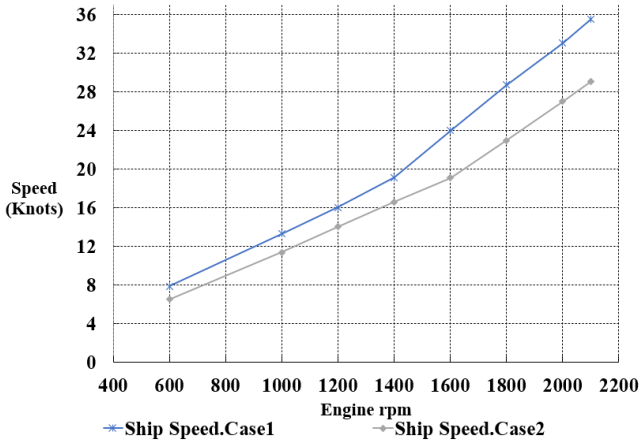

Figure 13. Prediction of the ship speed at engine speed in two cases

Figure 14 presents the values of Kt and Kq for the three-ship speeds of 23.6, 27, and 29 knots.

Table 8. Prediction of the top Speed at the four Cases

Case No.	Gear. R	V_s (knots)
Case1	2.571:1	23.6
Case2	2.963:1	۲۹

The efficiency of the propulsion system is shown in Figure 15 for the two cases. The propulsion efficiency is presented at several speeds of the engine from 600 to 2100 rpm. The propulsion efficiency in top speed of the ship for case 1and case 2 are found 61% and 61.8%, respectively.

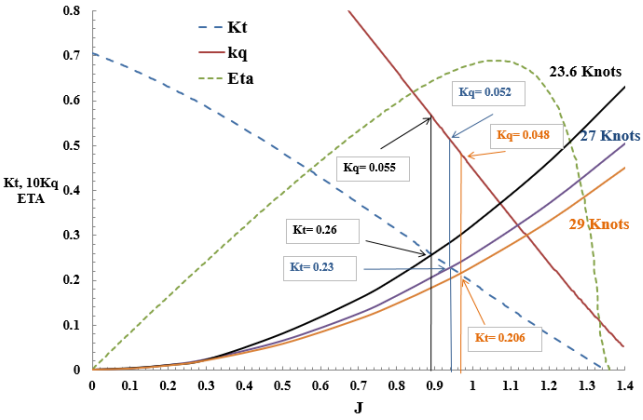

Figure 14. Kt, Kq, Eta, J diagram of propeller

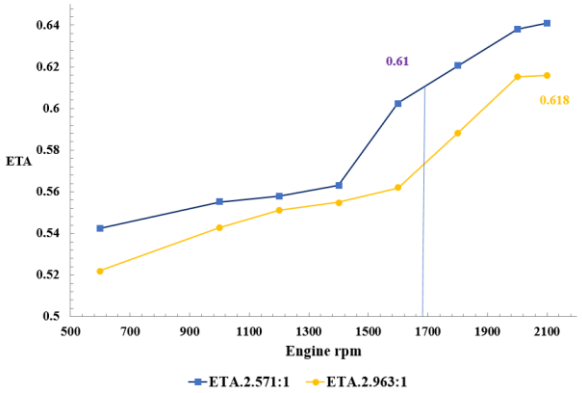

Figure 15. Prediction of the ship speed at engine speed in two cases

As shown in Fig 15, the efficiency graph is close to each other as engine speed goes up to 1400 rpm; and then moves away from each other. This behavior was also observed in the ship speed graph in Figure 13. This indicates the optimal performance of the propeller at speeds above 500 rpm.

Figure 16 shows the power of acceleration reserve in the four cases and the propeller theoretical power. The power of acceleration reserve shows the vertical distance of design propeller power and engine overload power. The vertical distance from the Acc.Rez.Case1 graph to the horizontal axis is less than the other one case. The points where these graphs intersect the horizontal axis where the overload occurs, and acceleration reserve power is zero. The Acc.Rez.Theoretical graph is a suitable measure for the acceleration reserve power. In Figure 16 it is compared with other graphs. This comparison shows that case 2 has the most suitable acceleration reserve power.

Fuel consumption is calculated at 1000 kW (60% rating power). Figure 17 shows BSFC graph of MTU12V396 and the design propeller power of two cases.

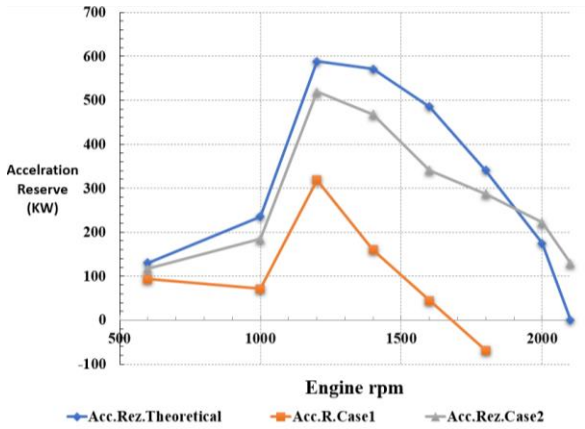

Figure 16. The Comparison of Reserved Acceleration in all cases

The brake specific fuel consumption graph of the engine has the lowest value near the overload power range and by moving away from it, their value increases. The design propeller power of case 1 and case 2 are intersected the average load line in the range of 204 g/kW.h and 206 g/kW.h of BSFC. The fuel consumption is obtained from power multiplied by BSFC. The density of the diesel fuel is 835 kg/m3 and the fuel consumption is presented in Table 9 in litters per hour.

Table 9. Fuel consumption at the two cases

Case No.	BSFC (g/kW.h)	Consumption (Litter/h)
Case 1	204	244
Case 3	206	246

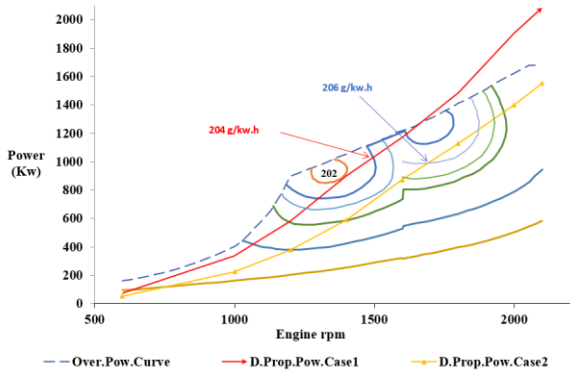

Figure 17. Brake Specific Fuel Consumption of MTU12V396 and design propeller power of the two cases

3.4. The second sea trial

The vessel is tested after changing the gearbox with a 2.963:1 of gear ratio. The results of the second sea trial are shown in Table 10.

Table 11 shows the engine performance characteristics at 1600 rpm and 2000 rpm of engine speed. By comparing the exhaust temperature row in Table 4 and Table 11, the exhaust temperature decreased on average at 148 °C at 1600 rpm in case 2. The maximum exhaust temperature has been 686°C at 2000 rpm which is natural and following the manufacturer's request.

Table 10. The Second Sea Trial Results

Engine rpm	Propeller rpm	Speed (knots)
600	202.5	7.2
1200	405	13
1400	472.5	16.5
1600	540	18.5
1800	607.5	22
2000	675	26.5
2100	708.7	28.5

The secondary turbocharger is activated at 1840 rpm in this case which shows that it has increased about 160 rpm more than in the case 1.

Table 11. Engine Performance Characteristics at 1600 and 2000 rpm in the Second See Trial

Test time	10:30		10:50	
	Port	Star board	Port	Star board
n_{enge} (rpm)	1600	1600	2000	2000
Tcoolant (° C)	78	78	79	79
Tex.combA (° C)	442	471	640	668
Tex.combB (° C)	448	483	686	655
Shaft Speed (rpm)	622	622	675	675
Speed (Knot)	18.5		26.5	

Figure 18 shows error bars for velocity prediction between the matching calculations and the second sea trial at 600 to 2100 rpm. The error value is from 4% to 7% and shows good accuracy in matching calculations.

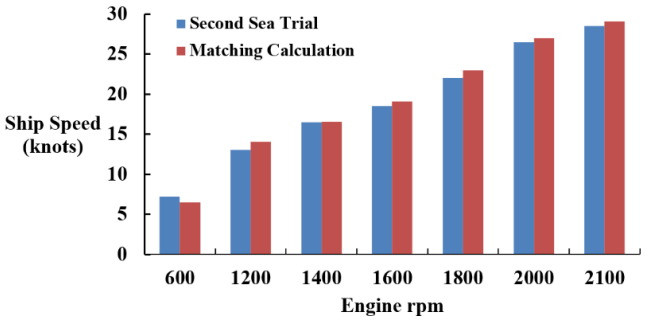

Figure 18. Velocity prediction error bars between the matching calculations of case 2 and the Second Sea Trial

4. Uncertainty Analysis

At these experiments, there are some error sources like any other measurements. The accuracy of sensors is the main error sources for the presented results. Vessel speed is measured with ±0.08 knot accuracy and the engine speed accuracy is also about ±10 rpm. The GPS model is Furuno, and the engine monitoring system is from MTU. The effect of these errors in the matching calculation of the second sea trial is investigated for minimum and maximum of engine speed and is presented in Table 12. In the item of error of GPS, only GPS error is calculated and in item of error of rpm,

only engine speed error is calculated and in the item of total error, the error of both is calculated simultaneously. The maximum error occurs at low engine speeds and high engine speeds, the error is less (where the top ship speed and ship service speed are calculated). Choosing regression formulas to calculate wake fraction and thrust deduction has a 2% error. Based on the uncertainty analysis calculations, the maximum error is 3.8%.

Table 12. Effect of GPS and engine rpm errors in matching calculation in the second sea trial

	Engine rpm	Speed (knots)	Error of GPS %	Error of rpm %	Total Error %
1	600	7.2	1.6	1.8	0.5
2	2100	28.5	0.3	1	0.2

5. Conclusion

This paper has investigated the propulsion system of a passenger catamaran ship. The matching condition of the propeller to the diesel engine and hull of the vessel for the two gear ratios of the gearbox has been analyzed. 2.963: 1 is selected as the gear ratio with 20 knots ship service speed and 29 knots top speed.

- Rating power of the engine is sufficient for a heavy condition at this gear ratio and the top speed reaches 29 knots.
- The design propeller power curve has been good following the propeller theoretical power at sea trial.
- The gearbox reduction ratio increased from 2.571:1 to 2.963:1 and the second sea trial is performed. Exhaust temperature decreased on average at 148°C at 1600 rpm in the case 2 (near the overload point in the first sea trial). In this engine, the secondary turbocharger is activated according to the engine load and is activated at 1840 rpm in this gear ratio. It has increased by about 160 rpm compared to the first sea trial. In case 2, the service speed of 20 knots was obtained in good conditions of engine operation such as brake specific fuel consumption (BSFC) and acceleration reserve. The operating conditions of the ship are satisfactory in terms of service speed, top speed, ship maneuverability power, and safe operation of the engine after changing the gearbox reduction ratio.

Symbol

n_{prop}	Propeller speed
P_b	Break power
P_D	Delivery Power
P_E	Effective Power
p	Pitch
$Prop.Pow$	propeller theoretical power
q	Torque
T	Thrust
$T.Ded$	Delivery Thrust
V_a	Advance Speed
V_s	Ship Speed

6. References

1- Woodward JB. Matching Engine and propeller. Univ., Department of Naval Architecture and Marine Engineering; 1976.

2- Marine Engines Application and Installation Guide. Caterpillar. 2000 Caterpillar Inc. Printed in U.S.A.

3- Samson N. World Journal of Engineering Research and Technology WJERT. World Journal of Engineering. 2017;3(1):161-77.

4- Grunditz G. Optimizing propeller and propulsion. The quest for reduced fuel consumption, emissions, and noise levels. Published in Marine Technology, January 2015. 2015.

5- Habibi, Nurhadi. Analysis of propeller type B-series selection on RO- RO 600 GT Ferry using Matchpro Application. Jurnal Ilmiah Teknologi Maritim Wave. Vol. 10 No.02; 2016. p. 75–81.

6- Abidin MZ, Adji SW. Analisa Performance Propeller B-series dengan pendekatan structure dan unstructure meshing. Jurnal Teknik ITS. 2012 Sep 11;1(1):G241-6.

7- Altosole M, Borlenghi M, Capasso M, Figari M. Computer-based design tool for a fuel efficient-low emissions marine propulsion plant. ICMRT Proceedings. 2007.

8- Pivano L. Thrust estimation and control of marine propellers in four-quadrant operations. Doctoral thesis. Fakultet for informasjonsteknologi, matematikk og elektroteknikk. 2008

9- Habibi, P., Nurhadi, H. 2016 Analysis of propeller type B- series selection on RO- RO 600 GT Ferry using Matchpro Application. J. Ilmiah Teknologi Maritim Wave. 10, 75–81.

10- Ogar OB, Nitonye S, John-Hope I. Design analysis and optimal matching of a controllable pitch propeller to the hull and diesel engine of a CODOG system. Journal of Power and Energy Engineering. 2018 Mar 29;6(03):53.

11- Nurhadi, Zen. H. Sumarsono. Study of Engine Propeller Matching for High-Speed Vessel with Gawn Series Propeller. EPI International Journal of Engineering. Vol. 1, No. 1, February 2018, pp. 39-42.

12- Gaggero S, Dubbioso G, Villa D, Muscari R, Viviani M. Propeller modeling approaches for off–design operative conditions. Ocean Engineering. 2019 Apr 15;178:283-305.

13- Pakian Bushehri M, Golbahar Haghighi MR. Experimental and numerical analysis of Hydrodynamic Characteristics of a surface piercing propeller mounted on high-speed craft. International Journal of Maritime Technology. 2021 Apr 10;15:79-91.
14- Bushehri MP, Haghighi MG. Propulsion System Matching Analysis of a Catamaran Passenger Ship by Changing the Gear Ratio. Iranian Journal of Science and Technology, Transactions of Mechanical Engineering. 2023 Mar;47(1):91-107.
15- Tran TG, Kim HC. A study on the matching problem of engine, propeller, and ship hull under actual service conditions. International Journal of Naval Architecture and Ocean Engineering. 2023 Jan 1;15:100538.
16- Tan Q, Sui C, Ding Y, Liu H, Gao C. Effect of Shaft System Arrangements on Ship-Engine-Propeller Matching. InInternational Conference on Marine Equipment & Technology and Sustainable Development 2023 Apr 1 (pp. 668-687). Singapore: Springer Nature Singapore.
17- Bayraktar M, Göksu B, Yüksel O. Matching of propulsion system components for a planing hull model. Ships and Offshore Structures. 2024 May 29:1-2.
18- Ramadhan BR, Purwana A. Investigating the Engine Propeller Matching of Triple Screw Ro-Ro Passenger Ship. In International Conference on Maritime Technology and Its Application 2025 Jan 17 (Vol. 1, No. 1, pp. 1-9).
19- Orca3D User Manual. Leveraging the power of Rhino for the naval architect. Version 1.3.4. © 2018-2024 by Orca3D
20- STAR CCM+. Product Version of Simcenter STAR-CCM+ Build 14.02.010. Documentation-version 2019.1. NY, USA.
21- Tezdogan T, Demirel YK, Kellett P, Khorasanchi M, Incecik A, Turan O. Full-scale unsteady RANS CFD simulations of ship behaviour and performance in head seas due to slow steaming. Ocean Engineering. 2015 Mar 15;97:186-206.
22- Khazaee R, Rahmansetayesh MA, Hajizadeh S. Hydrodynamic evaluation of a planing hull in calm water using RANS and Savitsky's method. Ocean Engineering. 2019 Sep 1;187:106221.
23- Molland AF, Turnock SR, Hudson DA. Ship resistance and propulsion. Cambridge university press; 2017 Aug 17.
24- MTU Diesel Engine. Operation and Manual of 12v396. © 2013 Copyright MTU Friedrichshafen, Rechtsform: GmbH. www.mtu-solutions.com.
25- LR. Rules and Regulation for the Classification of Ships. Part 5 Main and Auxiliary engine. July 2016